^{19}F Fast Magic-Angle Spinning NMR Spectroscopy on Microcrystalline Complexes of Fluorinated Ligands and the Carbohydrate Recognition Domain of Galectin-3

Roza Kalabekova[1], Caitlin M. Quinn[1], Kumar Tekwani Movellan[1], Angela M. Gronenborn[1,2*], Mikael Akke[3*], Tatyana Polenova[1,2*]

[1]Department of Chemistry and Biochemistry, University of Delaware, Newark, DE 19716, United States;
[2]Department of Structural Biology, University of Pittsburgh School of Medicine, 3501 Fifth Ave., Pittsburgh, PA 15261, United States;
[3]Division of Biophysical Chemistry, Center for Molecular Protein Science, Department of Chemistry, Lund University, P.O. Box 124, SE-22100 Lund, Sweden

ABSTRACT

Structural characterization of protein-ligand binding interfaces at atomic resolution is essential for improving the design of specific and potent inhibitors. Herein, we explored fast ^{19}F- and ^{1}H-detected magic angle spinning NMR spectroscopy to investigate the interaction between two fluorinated ligand diastereomers with the microcrystalline galectin-3 carbohydrate recognition domain. The detailed environment around the fluorine atoms was mapped by 2D ^{13}C-^{19}F and ^{1}H-^{19}F dipolar correlation experiments and permitted characterization of the binding interface. Our results demonstrate that ^{19}F MAS NMR is a powerful tool for detailed characterization of protein-ligand interfaces and protein interactions at the atomic level.

KEYWORDS ^{19}F magic angle spinning nuclear magnetic resonance, MAS NMR, ^{1}H-detected fast MAS, protein-ligand interactions, galectin-3C

INTRODUCTION

Interactions between proteins and small-molecule ligands play crucial roles in all biology, such as receptor signaling pathways and metabolic regulatory networks.[1-4] Atomic-level characterization of these interactions is essential for understanding the underlying mechanisms and for the design of specific inhibitors to interfere with these processes.[5-7] NMR spectroscopy is a powerful technique for investigating structural and dynamic aspects of protein-ligand interactions, both in solution and in the solid state.[8-11] To study protein-ligand complexes by NMR, ^{13}C, ^{15}N, and ^{1}H nuclei are most often used as reporters, exploiting isotopically enriched proteins or ligands. ^{19}F, a spin-1/2 nucleus, has excellent NMR properties: 83% sensitivity compared to ^{1}H, with chemical shifts exquisitely sensitive to local chemical and electronic environments over a range of ~300 ppm.[12, 13] ^{19}F MAS NMR has already gained importance as an informative technique for structural analysis of proteins, protein complexes, and small-molecule pharmaceuticals.[14-26] However, surprisingly, only few MAS NMR structural studies of protein complexes with fluorinated ligands have been reported.[27, 28] Here, we present proof of concept for ^{19}F fast MAS NMR correlation spectroscopy as a general approach for probing protein-ligand interfaces, using the microcrystalline carbohydrate binding domain consisting of residues P113-I250, of galectin-3 (galectin-3C, UniProt P17931), referred to as galectin-3C, complexed with galactose-derived fluorinated binders.

Galectins are a family of carbohydrate-binding proteins defined by a conserved recognition domain that binds β-D-galactopyranoside.[29] Of the 14 known mammalian galectins,[30] galectin-3 has been extensively studied, given its roles in apoptosis,[31-33] cancer progression,[34-36] and immune regulation.[37-39] Overexpression of galectin-3 in tumors[32, 40-42] afforded the initial motivation for inhibitor development of galectin-3C as anticancer agents,[43-45] although high toxicity thwarted their therapeutic use. Structural investigations of galectin-3C identified an extended pocket that can accommodate longer sugar-based molecules,[46, 47] and targeting this pocket in order to improve specificity and reduce toxicity is actively pursued, with thiogalactoside and thiodigalactoside derivatives containing triazolyl moieties possessing improved binding selectivity towards this extended binding pocket.[48]

Previous in-depth investigations of the thermodynamics of ligand binding to galectin-3C (Figure 1a,c) integrated experimental and computational methods, including isothermal titration calorimetry, X-ray crystallography, NMR spectroscopy, molecular dynamics simulations, and grid inhomogeneous solvation theory (GIST) analyses.[49] These studies revealed that variations in thermodynamic properties of galectin-3C complexes with diastereomeric ligands, such as (2R)- and (2S)-2-hydroxy-3-(4-(3-fluorophenyl)-1H-1,2,3-triazol-1-yl)-propyl) 2,4,6-tri-O-acetyl-3-deoxy-3-

(4-(3-fluorophenyl)-1H-1,2,3-triazol-1-yl)-1-thio-β-d-galactopyranoside (denoted as ligands R and S, Figure 1b), involve a complex interplay between protein conformational entropy and solvation entropy that contributes to the binding differences in the two complexes.[49] The binding affinities of the two fluorinated diastereomeric thio-β-d-galactopyranoside derivatives (S and R) to galectin-3C are 2.1 ± 0.1 and 1.0 ± 0.03 μM for the galectin-3C/S and galectin-3C/R complexes, respectively.[49] for bothTo complement and further investigate the forces governing ligand affinity differences, structural details of the ligand interactions with the protein binding sites need to be assessed. Therefore, we further examined microcrystalline galectin-3C complexes with lactose, S and R ligands, for which high-resolution X-ray structures are available (Figure 1) by ^{19}F MAS NMR.[49, 50]

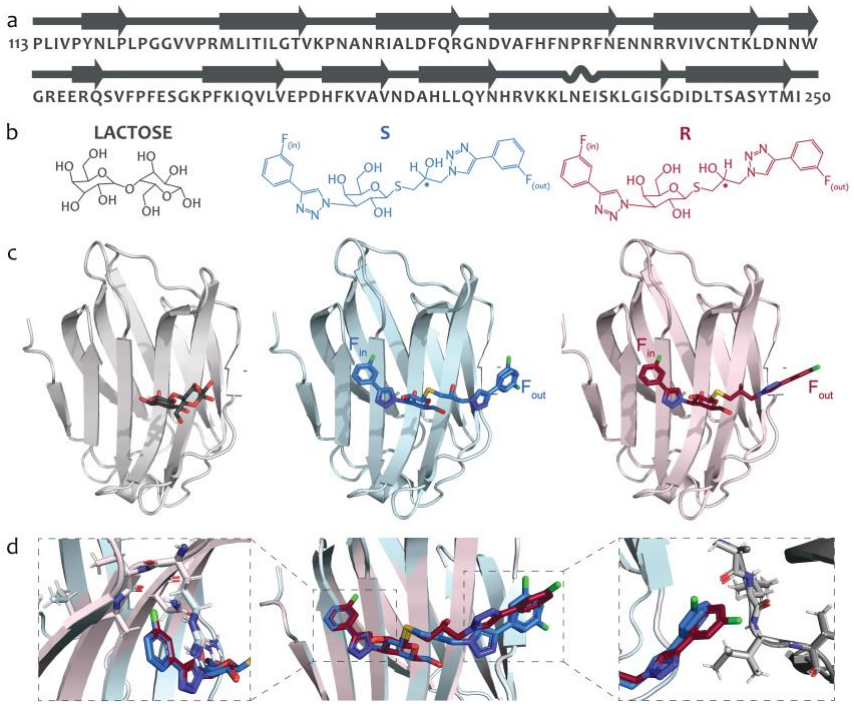

Figure 1. a) Amino acid sequence of galectin-3C. b) Chemical structures of lactose (grey), S (blue), and R (red). c) Ribbon representation (grey) of the X-ray structures of galectin-3C in complex with lactose (PDB ID: 3ZSJ, 0.86 Å resolution) and fluorinated diastereomeric ligands S (blue) (PDB ID: 6QGE, 1.16 Å resolution) and R (red) (PDB ID: 6QGF, 1.34 Å resolution). d) The structures of S (blue) and R (red) ligands bound to galectin-3C are superimposed . Details of the F_{in} and F_{out} interactions with galectin-3C amino acid side chains are shown in the left and right panels, respectively.

Judicious combinations of ^{1}H-^{19}F and ^{13}C-^{19}F dipolar correlation experiments, in conjunction with 2D and 3D ^{1}H-detected spectra yielded remarkably rich information about the details of the galectin-3C interactions with two very similar fluorinated ligands, demonstrating the power of fast ^{19}F MAS NMR spectroscopy for in-depth characterization of the protein-ligand interface. Overall, our

methodology is applicable to any protein complexes with fluorinated ligands, does not rely on protein deuteration, and thus represents a general strategy to investigate a broad range of systems.

RESULTS AND DISCUSSION

Galectin-3C chemical shifts: assignments and ligand-induced perturbations

The backbone resonances of galectin-3C were assigned using a combination of ^{1}H-detected 3D (H)CANH, (H)CONH, and (H)(CO)CA(CO)NH spectra, and the 2D (H)NH and (H)CH spectra of the galectin-3C/lactose complex. The 2D projections derived from these spectra are presented in Figure S1. Given the high spectral resolution and sensitivity for the microcrystalline galectin-3C/lactose sample, the backbone ^{1}H, ^{13}C, and ^{15}N chemical shifts could be unambiguously determined for 117 out of 138 galectin-3C residues.

The 3D ^{1}H-detected (H)CANH MAS NMR spectra of the fully protonated galectin-3C/lactose, galectin-3C/R, and galectin-3C/S complexes exhibit high resolution, as illustrated in an overlay of the two 2D NCA projections from the 3D (H)CANH spectra in Figure 2. The ^{13}C and ^{15}N chemical shifts for the galectin-3C/lactose and galectin-3C/S complexes are virtually identical, while small but pronounced differences were observed for several residues in galectin-3C/S and galectin-3C/R complexes, shown in the insets in Figure 2b.

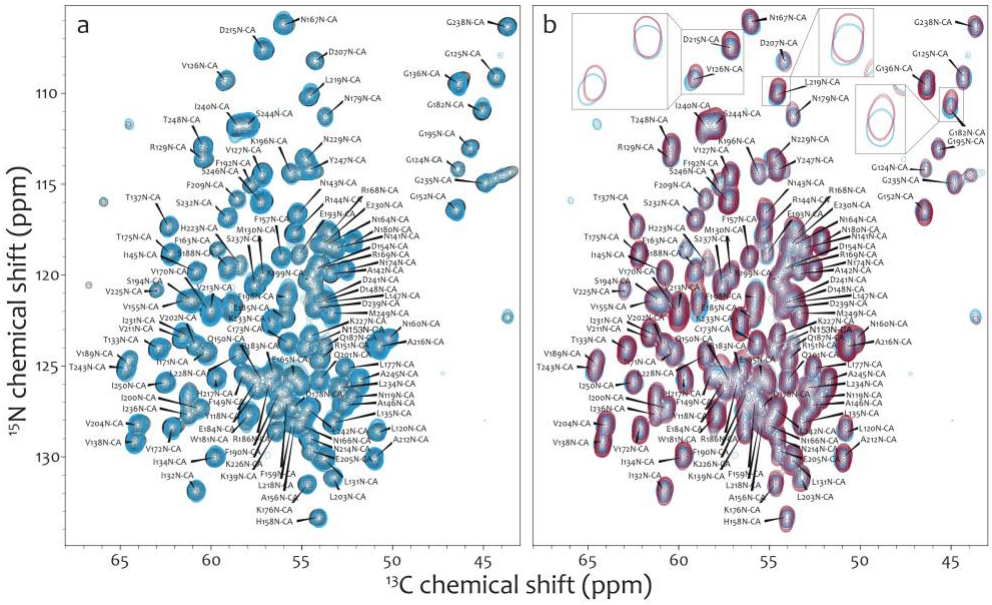

Figure 2. 2D NCA projections from the 3D ^{1}H-detected (H)CANH spectra shown as an overlay for a) galectin-3C/lactose (grey) and galectin-3C/S (blue), and b) galectin-3C/S (blue) and galectin-3C/R (red) complexes; residues with the largest chemical shift changes are boxed and expanded in the insets. The spectra were acquired at 20.0 T with a MAS frequency of 60 kHz.

To further investigate chemical shift differences between galectin-3C/lactose and galectin-3C/R complexes, 3D RN-symmetry driven CSA recoupling (RNCSA) experiments[51, 52] were recorded to derive residue-specific ^{15}N chemical shift anisotropy (CSA) tensors. The ^{15}N CSA provides information about the electronic environment and local structure around the nitrogen atoms, which may aid in understanding the source of chemical shift changes, such as conformational dynamics and

structural heterogeneity. In Figure 3, ^{15}N RNCSA line shapes are shown for residues exhibiting the largest ^{15}N chemical shift perturbations (CSPs) for galectin-3C bound to ligand R vs. S and lactose, such as V126, G182, D215, and L219. The corresponding CSA parameters are summarized in Table 1. All these residues are located in the loops and/or on the outer surface of galectin-3C and no structural differences for these residues are observed in the X-ray structures, as illustrated in Figure S2. Interestingly, the ^{15}N CSA tensors for galectin-3C residues in the ligand binding pocket do not exhibit any significant differences, as shown in Figure S3 and Table S1, indicating that the fluorinated moieties of the ligands do not perturb the electronic environment of protein residues within the binding site.

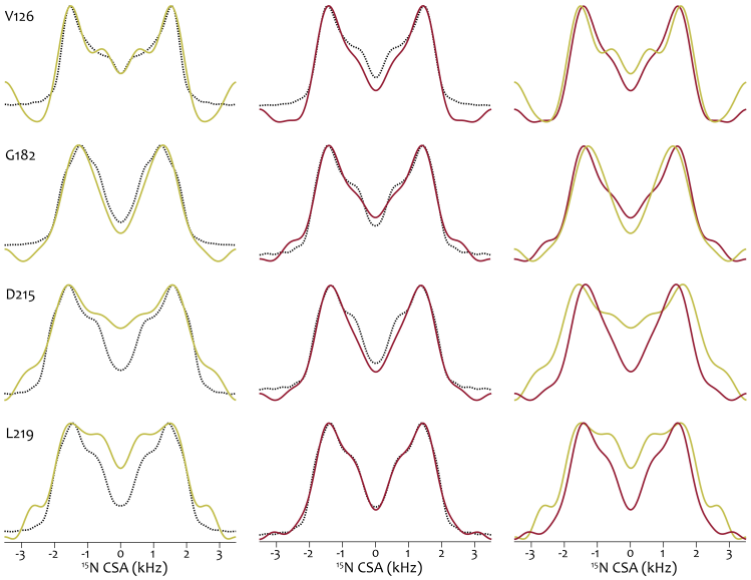

Figure 3. Overlay of the experimental (solid line) and simulated (dashed line) ^{15}N CSA lineshapes for galectin-3C/lactose (yellow) and galectin-3C/R (red) residues exhibiting the largest isotropic chemical shift differences between the two complexes(left and middle). Overlay of the experimental ^{15}N CSA lineshapes for galectin-3C/lactose (yellow) and galectin-3C/R (red) complexes (right).

Table 1. ^{15}N chemical shift anisotropy parameters for galectin-3C/lactose and galectin-3C/R residues with the largest chemical shift differences between the two complexes.

galectin-3C complex	V126		G182		D215		L219	
	δ_σ(ppm)	η	δ_σ(ppm)	η	δ_σ(ppm)	η	δ_σ(ppm)	η
lactose	90±11	0.2	82±8	0.7	95±16	0.5	93±21	0.5
R	87±4	0.3	87±1	0.4	86±5	0.5	88±1	0.5

^{19}F-based MAS NMR experiments to probe galectin-3C binding interfaces with fluorinated ligands

Chemical shift assignment and ligand-protein correlations: 1D ^{19}F MAS NMR spectra of galectin-3C/S and galectin-3C/R complexes acquired at a MAS frequency of 60 kHz are shown in Figure 4. Two well-resolved resonances are present in each ^{1}H decoupled spectrum, with isotropic chemical shifts of -34.9 ppm and -35.4 ppm for the galectin-3C/S complex, and -34.8 ppm and -35.2 ppm for the galectin-3C/R complex. Thus, each fluorine atom in the S and R molecules gives a rise to a distinct peak. Without ^{1}H decoupling, the two peaks are unresolved (Figure S4). The spectra exhibit high sensitivity and spectral resolution, despite the low amount of ^{19}F in each sample (~ 0.2% (w/w), 0.5 µmoles of ^{19}F for galectin-3C/S complex; ~ 2.6% (w/w), 0.25 µmoles of ligand for galectin-3C/R complex), and were recorded in three and five hours, respectively.

Despite the identical sample preparation protocols and NMR experimental conditions, the two galectin-3C bound ligand resonances exhibit slightly different line widths. The deshielded resonances at δ_{iso} = -34.9 and -34.8 ppm possess line widths of 0.3 and 0.2 ppm in the galectin-3C/S and galectin-3C/R spectra, respectively, while the corresponding values for the shielded peaks at δ_{iso} = -35.4 and -35.2 ppm are 0.2 and 0.3 ppm. These values and the longitudinal relaxation times (T_1) are summarized in Table 2.

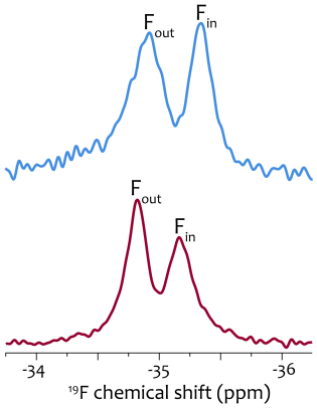

Figure 4. ^{19}F MAS NMR spectra of the galectin-3C/S complex (top) and the galectin-3C/R complex (bottom) acquired at 11.7 T with a MAS frequency of 60 kHz.

Table 2. Summary of ^{19}F MAS NMR spectral parameters and longitudinal relaxation time.

	galectin-3C/S				galectin-3C/R			
	δ_{iso} (ppm)	Line width (Hz/ppm)	T_1 (s)	SNR[a]	δ_{iso} (ppm)	Line width (Hz/ppm)	T_1 (s)	SNR[a]
F_{in}	-35.4	112/0.2	3.0	22	-35.2	132/0.3	3.4	30
F_{out}	-34.9	163/0.3	1.0	20	-34.8	100/0.2	1.1	40

[a]Signal-to-noise ratio

The narrowest peak is observed for the resonance at -34.8 ppm in the galectin-3C/R complex, assigned to the fluorophenyl moiety (see below) away from the binding site (F_{out}), while the corresponding peak in the galectin-3C/S displays the largest line width. Interestingly, a previous molecular dynamics (MD) simulation study revealed motion and disorder in the part of the S ligand that is outside the binding site.[49] The B factors of the F_{out} atom (20–35 Å^2 in the galectin-3C/R and 20–40 Å^2 in the galectin-3C/S) were higher than those of the F_{in} atoms (10–15 Å^2 in both complexes), indicating that F_{in} is more ordered.[49] Consistent with the larger B factor values is the observed line broadening of the deshielded peak in the galectin-3C/S complex, compared to the equivalent peak in the galectin-3C/R complex.

To define the interfaces of galectin-3C with ligands S and R, we conducted 2D dipolar-based correlation experiments. The (^{1}H)^{13}C-^{19}F and ^{1}H-^{19}F HETCOR spectra of the two complexes are presented in Figure 5, alongside a 2D ^{1}H-^{13}C HETCOR spectrum of the galectin-3C/lactose complex for reference.

The assignments of ^{13}C chemical shifts and intramolecular ^{13}C-^{19}F correlations were carried out with the assistance of the 3D and 2D ^{1}H-detected MAS NMR spectra discussed above, as well as the 2D CORD spectra reported in our previous study on the galectin-3C/lactose complex chemical shifts.[53] For assigning the ^{1}H chemical shifts and the intermolecular ^{1}H-^{19}F correlations we took advantage of 2D CORD,[53] 3D ^{1}H-detected (H)CCH, and 2D (H)CH HETCOR spectra of the galectin-3C/lactose sample. These spectra were processed for both sensitivity and resolution, to facilitate the unambiguous assignment of ^{13}C-^{19}F correlations in the extended pocket of the galectin-3C/S and galectin-3C/R complexes.

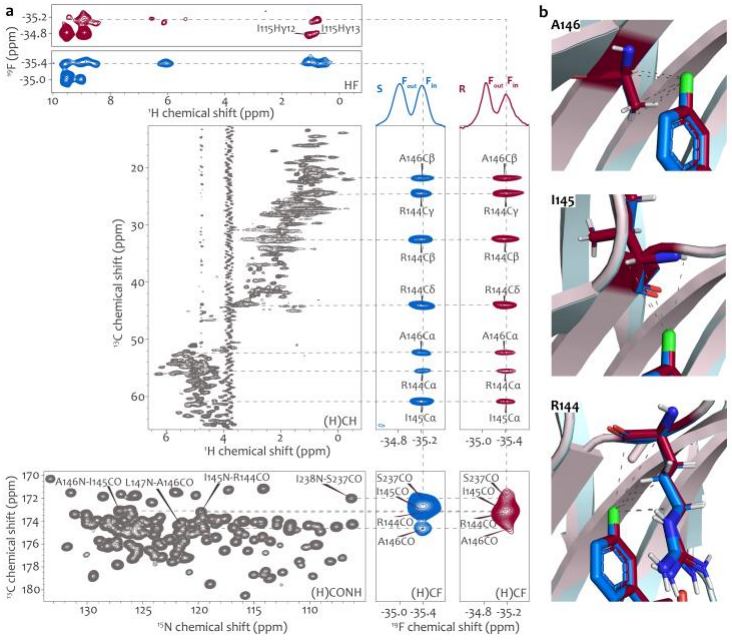

Figure 5. a) Top: 2D ^{1}H-^{19}F HETCOR spectra of the galectin-3C/S (blue) and galectin-3C/R (red) complexes, collected with a cross polarization (CP) contact time of 1 ms. Spectra were acquired at 11.7 T with a MAS frequency of 60 kHz. Middle left: ^{1}H-detected 2D (^{1}H)^{13}C-^{1}H HETCOR spectrum of the galectin-3C/lactose complex, acquired at 20.0 T with a MAS frequency of 60 kHz. Middle and bottom right: 2D (^{1}H)^{13}C-^{19}F HETCOR spectra of galectin-3C/S (blue) and galectin-3C/R (red) complexes, recorded with a ^{13}C-^{19}F CP contact time of 2 ms. The 1D ^{19}F spectra are displayed at the top of the 2D (^{1}H)^{13}C-^{19}F traces. Spectra were acquired at 11.7 T with a MAS frequency of 60 kHz. Bottom left: 2D NCO projection spectrum of the ^{1}H-detected 3D (H)CONH spectrum of the galectin-3C/lactose complex, recorded at 20.0 T with a MAS frequency of 60 kHz. b) Protein residues corresponding to the ^{19}F-^{13}C interactions with Fin in the binding pockets of galectin-3C are shown for the galectin-3C/S (cyan/blue) and galectin-3C/R (pink/red) complexes.

The most prominent cross peaks observed in the (^{1}H)^{13}C-^{19}F spectra of the galectin-3C complexes with S and R correspond to protein-ligand correlations between the F_{in} resonance of the ligand and the C' resonance of I145 of galectin-3C. The corresponding atoms are separated by 3 Å and 3.1 Å in the galectin-3C complexes with ligands S (PDB ID: 6QGE) and R (PDB ID: 6QGF), respectively. The least intense ^{13}C-^{19}F correlation is to A146(C'), corresponding to an interatomic distance of 5.3 Å in both complexes. The cross peaks between the resonance of F_{in} and those of A146(C^{β}) and R144(C^{γ}) in the (^{1}H)^{13}C-^{19}F HETCOR spectra for the galectin-3C/R complex are broadened in the ^{19}F dimension (Figure 5), indicating conformational heterogeneity. This agrees with findings in the X-ray structure and MD simulations that showed multiple side chain orientations of the R144 residue and enhanced motions in the galectin-3C/R complex.[49] A summary of the ^{19}F linewidths for all well-resolved correlations in the (^{1}H)^{13}C-^{19}F HETCOR spectra is provided in Table 3. As discussed above, no cross peaks were observed between the F_{out} resonance and other resonances in spectra of either complex, consistent with the fluorophenyl location distal from the binding site.

Table 3. Summary of ^{19}F linewidths in 2D (^{1}H)^{13}C-^{19}F HETCOR spectra of galectin-3C/S and galectin-3C/R complexes

	galectin-3C/S (Hz/ppm)	galectin-3C/R (Hz/ppm)
A146(C^{β})	105/0.2	116/0.2
R144(C^{γ})	97/0.2	114/0.2
R144(C^{β})	113/0.2	102/0.2
R144(C^{δ})	101/0.2	102/0.2
A146(C^{α})	101/0.2	105/0.2
R144(C^{α})	103/0.2	133/0.3
I145(C^{α})	103/0.2	100/0.2

Additional insights into the binding interfaces were obtained from ^{1}H-^{19}F HETCOR spectra that exhibited both inter- and intramolecular correlations (Figure 5). Cross peaks are present correlating both fluorine resonances (F_{in} and F_{out}) to proton resonances with $\delta_{iso}(^{1}H)$ in the 8.5 ppm to 10 ppm range, arising most likely from intramolecular close contacts between the fluorine atoms and the aromatic protons of the ligands. The spectra also contain multiple intermolecular protein-ligand correlations. While most of the cross peaks belong to galectin-3C resonances observed in the (^{1}H)^{13}C-^{19}F HETCOR spectra, some additional intra- and inter-residue correlations between amide backbone and guanidinium side chain proton resonances are seen (Figure S5). Specifically, correlations to N160($H^{N\delta 2}$), R144($H^{N\eta 2}$), R144($H^{N\varepsilon}$), and I145(H^{N}), are observed, corresponding to internuclear distances of 3.4 to 6.2 Å.

The ^{1}H-^{19}F HETCOR spectra of the two complexes are distinctly different (Figure 5). A unique ^{19}F-^{1}H intermolecular correlation between F_{out}, the ^{19}F resonance of the aromatic moiety pointing away from the binding site, was noted in the 2D ^{19}F-^{1}H HETCOR spectrum of the galectin-3C/R complex, which is absent in the corresponding spectrum of the complex with S (Figure 5). We assigned this to a contact between F_{out} and I115 ($H^{\gamma 12}$ and $H^{\gamma 13}$) in the adjacent protein chain in the crystal (Figure 6). This result is in agreement with the observed differences in the galectin-3C/S and galectin-3C/R X-ray structures that show different conformations in the distal part of the ligand, including altered relative orientations of the fluorophenyl aromatic moieties and unique local environments (Figure 6). Thus, differences of this kind are detected with high sensitivity in the MAS NMR spectra. Overall, the present results validate the observed changes in the ensemble-refined X-ray structures, where the R ligand shows much lower fluctuations than S.

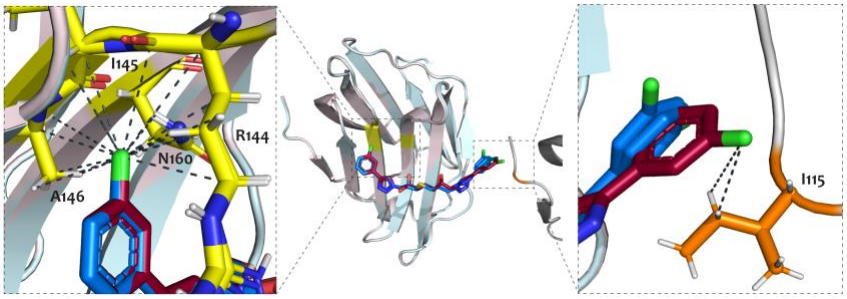

Figure 6. ^{19}F-^{13}C and ^{19}F-^{1}H contacts in the binding pockets of galectin-3C in the galectin-3C/S (cyan/blue) and galectin-3C/R (pink/red) complexes. Interactions involving F_{in} and galectin-3C residues surrounding the buried ligand moiety are shown in yellow stick representation (left). Contacts between F_{out} and the side chain of I115 (in orange stick representation) in the adjacent protein chain of the crystal (right). The enlarged regions are indicated in the full structure (middle).

^{19}F CSA parameters: To gain additional insights into the local environments of the fluorine moieties of the two ligands when bound to galectin-3C, we measured the ^{19}F CSA parameters by

recording the spectra at a MAS frequency of 10 kHz. As seen in Figure S6, the spinning side band manifolds are well defined, and we extracted the CSA parameters, reduced anisotropy (δ_σ) and asymmetry parameter (η) by fitting the experimental data using the solid line shape analysis module (sola) in TopSpin 4.1.3. The CSA parameters are summarized in Table 4.

Table 4. ^{19}F CSA parameters in the galectin-3C/S and galectin-3C/R complexes.

	galectin-3C/S			galectin-3C/R		
	δ_{iso} (ppm)	δ_σ (ppm)	η	δ_{iso} (ppm)	δ_σ (ppm)	η
F_{in}	-35.4	57	0.6	-35.2	57	0.6
F_{out}	-34.9	37	0.9	-34.8	37	0.9

For both complexes, the deshielded resonances (-34.9 and -34.8 ppm for galectin-3C/S and galectin-3C/R, respectively) are associated with δ_σ = 37 ppm, a much smaller chemical shift anisotropy compared to δ_σ = 57 ppm seen for the shielded peaks (-35.4 and -35.2 ppm for galectin-3C/S and galectin-3C/R, respectively). The observed reduction of δ_σ is indicative of dynamic averaging of the CSA tensor, through aromatic ring flips occurring on timescales of milliseconds and faster.[54] Indeed, the F_{out} site is solvent exposed and the corresponding aromatic ring can undergo 2-fold jumps resulting in ^{19}F CSA tensor averaging. In contrast, the F_{in} site is buried, interacts extensively with protein residues, and the aromatic ring jumps are hindered. The presence of aromatic ring flips in F_{out} is also evident in the two F_{out} conformations in the crystal structure. These results further support the assignment of the deshielded fluorine atom void of cross peaks in 2D ^{19}F-^{13}C HETCOR spectra (Figure 5) as F_{out}, distal from the binding site.

In summary,^{19}F MAS NMR enabled detailed structural characterization of the binding interfaces in galectin-3C complexes with two different fluorinated ligands. Unambiguous identification of protein-ligand correlations in the spectra was achieved through a combination of 2D ^{19}F dipolar-based correlation experiments at high spectral resolution. Moreover, the experiments reported herein helped to distinguish details of intermolecular ^{19}F-^{1}H correlations specific to each of the two diastereomers and report on the differences in the protein interactions with the respective ligands. While X-ray crystallography has provided structures for the galectin-3C complexes with the fluorinated ligands, NMR spectroscopy yields complementary insights about local electronic environment and dynamics of ligands as well as the protein using chemical shift and dipolar coupling tensors as exquisitely sensitive reporters. While the current study was performed at the MAS frequencies of up to 60 kHz, we anticipate that faster spinning, with frequencies of 100 kHz and

higher, will be advantageous and enable correlation experiments inaccessible with lower frequencies, as demonstrated by us recently.[55, 56] Together, our results highlight the power of ^{19}F fast-MAS NMR spectroscopy for investigating protein-fluorinated ligand interactions and provide a toolkit for a broad range of systems, beyond the specific example used here. Finally, we envision that similar approaches will find broad applications for improving existing ligands by guided drug design in a variety of biotechnology and pharmaceutical applications.

EXPERIMENTAL SECTION

Sample preparation

The carbohydrate recognition domain consisting of residues P113-I250, of galectin-3 (galectin-3C) was recombinantly expressed in isotopically (U-^{13}C, ^{15}N) enriched medium and purified by the Lund Protein Production Platform (LP3) at Lund University as described previously.[49, 57, 58] Three samples of galectin-3C complexes were prepared at Lund University by adding galectin-3C to lactose and two diastereomeric compounds (2R)- and (2S)-2-hydroxy-3-(4-(3-fluorophenyl)-1H-1,2,3-triazol-1-yl)-propyl) 2,4,6-tri-O-acetyl-3-deoxy-3-(4-(3-fluorophenyl)-1H-1,2,3-triazol-1-yl)-1-thio-β-d-galactopyranoside, denoted ligands R and S, respectively.49

Crystallization of the complexes were performed as described previously.[49] For MAS NMR experiments, microcrystals of galectin-3C/lactose, galectin-3C/S and galectin-3C/R, were ultracentrifuged into 1.3 mm rotors. Final amounts for the three samples were: 3.9 mg (galectin-3C/lactose), 4.1 mg (galectin-3C/S), and 4.1 mg (galectin-3C/R), respectively.

MAS NMR spectroscopy

2D and 3D ^{1}H-detected experiments were recorded on a 20.0 T Bruker AVIII spectrometer outfitted with a 1.3 mm HCN probe at 850.4 MHz (^{1}H), 213.9 MHz (^{13}C), and 86.2 MHz (^{15}N). ^{1}H-detected MAS NMR experiments were recorded at the MAS frequency of 60 kHz, controlled to within ±10 Hz by a Bruker MAS controller, and the sample temperature was maintained at ~25 ºC throughout the experiments. Typical 90° pulse lengths were 1.4-1.5 µs for ^{1}H, 2.9-3.1 µs for ^{13}C, and 3.0-3.2 µs for ^{15}N. Swept-low power TPPM (15 kHz slTPPM)[59] was used for ^{1}H-heteronuclear decoupling during acquisition. 10 kHz WALTZ-16[60] broadband decoupling was used for ^{13}C and ^{15}N decoupling during ^{1}H acquisition.

The 3D ^{1}H-detected (H)CONH spectra of microcrystalline U−^{13}C,^{15}N−galectin-3C/lactose were recorded with a 20% linear amplitude ramp on ^{15}N. The center of the ramp was Hartmann−Hahn matched to the first spinning sideband. For the forward (HC) CP and back (NH) CP, the radio frequency (RF) field strengths were 103 kHz for ^{1}H and 19 kHz for ^{13}C, and 118 kHz for ^{1}H and 41 kHz for ^{15}N, respectively. The CP contact times were 5 ms (HC) and 275 µs (NH). For the CN CP, a constant-amplitude spin lock of about 35 kHz on ^{13}C and a tangent-modulated amplitude spin lock of mean RF field amplitude of about 27 kHz on ^{15}N[61] were used. The CN CP contact time was 12 ms.

The 3D ^{1}H-detected (H)(CO)CA(CO)NH spectra of microcrystalline U−^{13}C,^{15}N−galectin-3C/lactose were recorded with 20% linear amplitude ramp on ^{15}N. The center of the ramp was Hartmann−Hahn matched to the first spinning sideband. For the forward (HC) CP, the RF field

strengths were 86 kHz on ^{1}H and 19 kHz on ^{13}C. For the back (NH) CP, the RF field strengths were 99 kHz on ^{1}H and 43 kHz on ^{15}N. The CP contact times were 5 ms (HC) and 300 μs (NH). For the CN CP, a constant-amplitude spin lock of about 35 kHz on ^{13}C and a tangent-modulated amplitude spin lock of mean RF field strength of about 27 kHz on ^{15}N were used. The CN CP contact time was 12 ms.

The 3D ^{1}H-detected (H)CANH spectra of microcrystalline U−^{13}C,^{15}N−galectin-3C/lactose, galectin-3C/S, and galectin-3C/R were recorded with 20% linear amplitude ramp on ^{15}N. The center of the ramp was Hartmann−Hahn matched to the first spinning sideband. For the forward (HC) CP, the RF field strengths were 99 kHz on ^{1}H and 19 kHz on ^{13}C. For the back (NH) CP, the RF field strengths were 128 kHz on ^{1}H and 43 kHz on ^{15}N. The CP contact times were 1.2 ms (HC) and 300 μs (NH). For the CN CP, a constant-amplitude spin lock of about 36 kHz on ^{13}C and a tangent-modulated amplitude spin lock of mean RF field amplitude of about 27 kHz on ^{15}N[61] were used. The CN CP contact time was 10 ms.

The 2D ^{1}H-detected (H)CH spectra were recorded with a 20% linear amplitude ramp on ^{1}H. The CP RF field strengths were 19 kHz for ^{13}C and 85 kHz for ^{1}H. The contact times were 1 ms and 200 μs, for HC and CH CP, respectively. The 3D (H)CCH spectra of microcrystalline U−^{13}C,^{15}N−galectin-3C/lactose were recorded with a 20% linear amplitude ramp on ^{1}H. The center of the ramp was Hartmann−Hahn matched to the first spinning sideband. The CP RF field strengths were 19 kHz for ^{13}C and 100 kHz for ^{1}H. The contact times were 2 ms and 500 μs, for HC and CH CP, respectively. The CC RFDR mixing time was 2.4 ms.

The 2D ^{1}H-detected (H)NH spectra were recorded with 20% linear amplitude ramp on ^{1}H. For the forward (HN) CP and back (NH) CP, RF field strengths were 130 kHz and 123 kHz for ^{1}H and 41 kHz and 41 kHz for ^{15}N, respectively. The contact times were 1.1 ms and 275 μs for HN and NH, respectively.

For all spectra, the ^{1}H RF field strengths for water suppression and proton decoupling were set at ¼ ω_r, and a WALTZ-16 sequence at 10 kHz was used for heteronuclear decoupling for both, ^{13}C and ^{15}N.

3D ^{1}H-^{15}N/^{13}C RNCSA experiments were recorded on a 20.0 T Bruker AVIII spectrometer equipped with 1.3 mm HCN probe. The spectra of microcrystalline U−^{13}C,^{15}N−galectin-3C/lactose and galectin-3C/R were collected at the MAS frequency of 14 kHz, controlled to within ±10 Hz by a Bruker MAS controller. The actual sample temperature was maintained at ∼25 ºC throughout the experiments. R14$^{2}_{5}$-based symmetry sequence was used to recouple the ^{1}H-^{15}N/^{13}C CSA interactions during t_1 evolution, and the phase alternating RF field irradiation (53 kHz) was applied on the ^{15}N channel.

1D and 2D (^{1}H)-^{13}C-^{19}F, ^{1}H-^{19}F) ^{19}F-detected MAS NMR spectra of U-^{13}C,^{15}N of galectin-3C/S and galectin-3C/R microcrystalline protein samples were recorded on a 11.7 T wide bore Bruker AVANCE III spectrometer outfitted with a 1.3 mm HFX MAS probe, the Larmor frequencies were 500.13 MHz (^{1}H), 470.59 MHz (^{19}F), and 125.76 MHz (^{13}C). The spectra were acquired at a MAS frequency of 60 kHz, controlled to within ±10 Hz by a Bruker MAS III controller, and the sample was maintained at ~28 °C by a Bruker variable temperature controller. The temperatures were calibrated using the T_1 relaxation time of ^{79}Br in KBr powder.[62] ^{19}F and ^{13}C chemical shifts were referenced with respect to trifluoroacetic acid (100 μM solution in 25 mM sodium phosphate buffer, pH 6.5) as an external reference (0 ppm) and adamantane (40.48 ppm), respectively. ^{1}H resonances were referenced to water at 4.7 ppm. ^{19}F and ^{1}H spin-lattice relaxation rates were measured using a standard inversion recovery sequence.[63] Typical 90° pulse lengths were 2.0 μs for ^{1}H, 2.4 μs for ^{19}F, and 3.2 μs for ^{13}C.

For the 2D (^{1}H)-^{13}C-^{19}F HETCOR experiments, ^{13}C–^{19}F cross-polarization was performed with a 20% linear amplitude ramp on ^{19}F and a CP contact time of 2 ms. The center of the ramp was Hartmann–Hahn matched to the first spinning sideband. The ^{13}C carrier frequency was set to 50 ppm. The ^{19}F and ^{13}C RF fields were 18 kHz and 42 kHz, respectively. For galectin-3C/S and galectin-3C/R 408 scans with 384 complex points and 256 scans with 496 complex points were acquired in the indirect (^{13}C) dimension, respectively. ^{19}F decoupling was performed with a rotor-synchronized π-pulse (RF field of 104 kHz) applied every second rotor period during evolution in the ^{13}C dimension. 15 kHz time-proportional phase modulation (TPPM)[59] ^{1}H decoupling was applied during acquisition.

For the 2D ^{1}H–^{19}F HETCOR experiments, ^{1}H–^{19}F cross-polarization was performed with a linear ramp. The typical ^{1}H and ^{19}F RF fields were 105 and 45 kHz, respectively. 408 scans with 128 complex points were acquired in the indirect (^{1}H) dimension for galectin-3C/S, and 152 scans with 128 complex points for galectin-3C/R, respectively. The CP contact times were 1 ms and 7 ms.

All experiment times are listed in the Supporting Information.

NMR data processing

NMR data processing was carried out in TopSpin and NMRpipe.[64] All 2D and 3D ^{1}H-detected data sets used for the backbone assignments were processed by applying 90° shifted sine bell apodization in all dimensions followed by a Lorentzian-to-Gaussian transformation in all dimensions. Each of the 2D ^{1}H-^{19}F and (^{1}H)^{13}C-^{19}F HETCOR spectra was processed in multiple ways by applying 30°, 45°, and 90° shifted sine bell apodization to highlight specific spectral characteristics, followed by a Lorentzian-to-Gaussian transformation in all dimensions. The ^{15}N RNCSA traces for individual

residues extracted from the 3D ^{1}H-^{15}N/^{13}C RNCSA spectra were processed using real Fourier Transform, to generate the respective frequency-domain line shapes.

Chemicals shift assignments

Spectra were analyzed using Sparky.[65] Galectin-3C/lactose backbone resonance assignments were carried out by using ^{1}H-detected 3D (H)CANH, (H)CONH, and (H)(CO)CA(CO)NH spectra and verified against previously reported MAS NMR chemical shifts.[53]

^{13}C and ^{1}H resonances in the (^{1}H)^{13}C-^{19}F and ^{1}H-^{19}F HETCOR spectra were assigned by inspection using the backbone assignments of the galectin-3C/lactose and (described above) and with the aid of ^{1}H-detected 3D (H)CCH and 2D (H)CH spectra as well as the previously reported assignments from ^{13}C-^{13}C correlations.[53]

The ^{19}F CSA parameters, reduced anisotropy (δ_σ) and asymmetry parameter (η) were extracted by fitting the experimental data using the TopSpin 4.1.3 solid lineshape analysis module (sola) using Simplex iterator. Fitting of ^{15}N CSA line shapes was performed using SIMPSON version 4.2.1 and the 'opt' package for fitting scripts.[66-68]

ACKNOWLEDGMENT

We thank Ulf J. Nilsson for contributing ligands and Olof Stenström for preparing samples of ligand-galectin-3C complexes. Protein production was carried out by the Lund Protein Production Platform (LP3) at Lund University.

ASSOCIATED CONTENT

Supporting Information Available:

Experimental procedures for sample preparation and MAS NMR spectroscopy; figures with ^{19}F MAS NMR spectra of galectin-3C/S without ^{1}H decoupling, 2D ^{1}H-^{19}F HETCOR spectra of galectin-3C/S. This material is available free of charge via the internet at http://pubs.acs.org.

AUTHOR INFORMATION

Corresponding Authors

*Tatyana Polenova – Department of Chemistry and Biochemistry, University of Delaware, Newark, Delaware 19716, United States; Pittsburgh Center for HIV Protein Interactions, University of Pittsburgh School of Medicine, Pittsburgh, Pennsylvania 15261, United States; orcid.org/0000-0002-0346-1131; Email: tpolenov@udel.edu

*Mikael Akke – Division of Biophysical Chemistry, Center for Molecular Protein Science, Department of Chemistry, Lund University, 221 00 Lund, Sweden; orcid.org/0000-0002-2395825X; Email: mikael.akke@bpc.lu.se

*Angela M. Gronenborn – Department of Structural Biology, School of Medicine, Department of Chemistry, Dietrich School of Arts and Sciences, Department of Bioengineering, Swanson School of Engineering, University of Pittsburgh, Pittsburgh, Pennsylvania 15261; Pittsburgh Center for HIV Protein Interactions; orcid.org/0000-0001-9072-3525; Email: amg100@pitt.edu

Author Contributions

T.P., M.A., A.M.G. conceived the project and guided the work. R. K., C. M. Q., and K. T. M. performed the NMR experiments. R. K. performed data analysis. R. K. and T. P. took the lead on writing the manuscript. All authors discussed the results and contributed to the manuscript preparation. All authors have given approval to the final version of the manuscript.

Funding Sources

This work was supported by the National Science Foundation (NSF Grant CHE-1708773 to A. M. G. and T. P.), by the National Institutes of Health (NIH Grant 1U54AI170791 to A. M. G., T. P., NMR Core), and by the Knut and Alice Wallenberg Foundation (KAW 2013.022 to M. A.), The Swedish Research Council (2018-4995).

Notes

The authors declare no competing financial interest.

References

1. Mannhold, R.; Kubinyi, H.; Folkers, G., *Protein-ligand interactions: from molecular recognition to drug design*. John Wiley & Sons: 2006.
2. Longo, F. M.; Massa, S. M., Small-molecule modulation of neurotrophin receptors: a strategy for the treatment of neurological disease. *Nat. Rev. Drug Discov.* **2013,** *12* (7), 507-525.
3. Wu, Q.; Jiang, L.; Li, S.-c.; He, Q.-j.; Yang, B.; Cao, J., Small molecule inhibitors targeting the PD-1/PD-L1 signaling pathway. *Acta Pharmacol. Sin.* **2021,** *42* (1), 1-9.
4. Kremer, D. M.; Lyssiotis, C. A., Targeting allosteric regulation of cancer metabolism. *Nat. Chem. Biol.* **2022,** *18* (5), 441-450.
5. Shinada, N. K.; de Brevern, A. G.; Schmidtke, P., Halogens in protein-ligand binding mechanism: a structural perspective. *J. Med. Chem.* **2019,** *62* (21), 9341-9356.
6. Vajda, S.; Beglov, D.; Wakefield, A. E.; Egbert, M.; Whitty, A., Cryptic binding sites on proteins: definition, detection, and druggability. *Curr. Opin. Chem. Biol.* **2018,** *44*, 1-8.
7. Garlick, J. M.; Mapp, A. K., Selective modulation of dynamic protein complexes. *Cell Chem. Biol.* **2020,** *27* (8), 986-997.
8. del Carmen Fernández-Alonso, M.; Díaz, D.; Alvaro Berbis, M.; Marcelo, F.; Jimenez-Barbero, J., Protein-carbohydrate interactions studied by NMR: from molecular recognition to drug design. *Curr. Protein Pept. Sci.* **2012,** *13* (8), 816-830.
9. Otting, G., Experimental NMR techniques for studies of protein-ligand interactions. *Curr. Opin. Struct. Biol.* **1993,** *3* (5), 760-768.
10. Maity, S.; Gundampati, R. K.; Suresh Kumar, T. K., NMR methods to characterize protein-ligand interactions. *Nat. Prod. Commun.* **2019,** *14* (5), 1934578X19849296.
11. Furukawa, A.; Konuma, T.; Yanaka, S.; Sugase, K., Quantitative analysis of protein–ligand interactions by NMR. *Prog. Nucl. Magn. Reson. Spectrosc.* **2016,** *96*, 47-57.
12. Sharaf, N. G.; Gronenborn, A. M., ^{19}F-modified proteins and ^{19}F-containing ligands as tools in solution NMR studies of protein interactions. *Methods Enzymol.* **2015,** *565*, 67-95.
13. Gerig, J., Fluorine NMR. *Biophysics Textbook Online* **2001**, 1-35.
14. Tengel, T.; Fex, T.; Emtenas, H.; Almqvist, F.; Sethson, I.; Kihlberg, J., Use of ^{19}F NMR spectroscopy to screen chemical libraries for ligands that bind to proteins. *Org. Biomol. Chem.* **2004,** *2* (5), 725-31.
15. Norton, R. S.; Leung, E. W.; Chandrashekaran, I. R.; MacRaild, C. A., Applications of ^{19}F-NMR in fragment-based drug discovery. *Molecules* **2016,** *21* (7).
16. Lu, M.; Ishima, R.; Polenova, T.; Gronenborn, A. M., ^{19}F NMR relaxation studies of fluorosubstituted tryptophans. *J. Biomol. NMR* **2019,** *73* (8-9), 401-409.
17. Matei, E.; Gronenborn, A. M., ^{19}F paramagnetic relaxation enhancement: a valuable tool for distance measurements in proteins. *Angew. Chem. Int. Ed. Engl.* **2016,** *55* (1), 150-4.
18. Danielson, M. A.; Falke, J. J., Use of ^{19}F NMR to probe protein structure and conformational changes. *Annu. Rev. Biophys. Biomol. Struct.* **1996,** *25*, 163-95.
19. Gilchrist, M. L., Jr.; Monde, K.; Tomita, Y.; Iwashita, T.; Nakanishi, K.; McDermott, A. E., Measurement of interfluorine distances in solids. *J. Magn. Reson.* **2001,** *152* (1), 1-6.
20. Roos, M.; Mandala, V. S.; Hong, M., Determination of long-range distances by fast magic-angle-spinning radiofrequency-driven ^{19}F-^{19}F dipolar recoupling NMR. *J. Phys. Chem. B* **2018,** *122* (40), 9302-9313.
21. Roos, M.; Wang, T.; Shcherbakov, A. A.; Hong, M., Fast magic-angle-spinning ^{19}F spin exchange NMR for determining nanometer ^{19}F-^{19}F distances in proteins and pharmaceutical compounds. *J. Phys. Chem. B* **2018,** *122* (11), 2900-2911.
22. Shcherbakov, A. A.; Roos, M.; Kwon, B.; Hong, M., Two-dimensional ^{19}F-^{13}C correlation NMR for ^{19}F resonance assignment of fluorinated proteins. *J. Biomol. NMR* **2020,** *74* (2-3), 193-204.

23. Shcherbakov, A. A.; Hong, M., Rapid measurement of long-range distances in proteins by multidimensional ^{13}C-^{19}F REDOR NMR under fast magic-angle spinning. *J. Biomol. NMR* **2018,** *71* (1), 31-43.
24. Fritz, M.; Kraus, J.; Quinn, C. M.; Yap, G. P. A.; Struppe, J.; Sergeyev, I. V.; Gronenborn, A. M.; Polenova, T., Measurement of accurate interfluorine distances in crystalline organic solids: a high-frequency magic angle spinning NMR approach. *J. Phys. Chem. B.* **2019,** *123* (50), 10680-10690.
25. Lu, M.; Sarkar, S.; Wang, M.; Kraus, J.; Fritz, M.; Quinn, C. M.; Bai, S.; Holmes, S. T.; Dybowski, C.; Yap, G. P. A.; Struppe, J.; Sergeyev, I. V.; Maas, W.; Gronenborn, A. M.; Polenova, T., ^{19}F magic angle spinning NMR spectroscopy and density functional theory calculations of fluorosubstituted tryptophans: integrating experiment and theory for accurate determination of chemical shift tensors. *J. Phys. Chem. B* **2018,** *122* (23), 6148-6155.
26. Wang, M.; Lu, M.; Fritz, M. P.; Quinn, C. M.; Byeon, I. L.; Byeon, C. H.; Struppe, J.; Maas, W.; Gronenborn, A. M.; Polenova, T., Fast magic-angle spinning ^{19}F NMR spectroscopy of HIV-1 capsid protein assemblies. *Angew. Chem., Int. Ed. Engl.* **2018,** *57* (50), 16375-16379.
27. Goetz, J. M.; Poliks, B.; Studelska, D. R.; Fischer, M.; Kugelbrey, K.; Bacher, A.; Cushman, M.; Schaefer, J., Investigation of the binding of fluorolumazines to the 1-MDa capsid of lumazine synthase by ^{15}N {^{19}F} REDOR NMR. *J. Am. Chem. Soc.* **1999,** *121* (33), 7500-7508.
28. Shcherbakov, A. A.; Spreacker, P. J.; Dregni, A. J.; Henzler-Wildman, K. A.; Hong, M., High-pH structure of EmrE reveals the mechanism of proton-coupled substrate transport. *Nat. Commun.* **2022,** *13* (1), 991.
29. Lajoie, P.; Goetz, J. G.; Dennis, J. W.; Nabi, I. R., Lattices, rafts, and scaffolds: domain regulation of receptor signaling at the plasma membrane. *J. Cell Biol.* **2009,** *185* (3), 381-5.
30. Hirabayashi, J.; Kasai, K., The family of metazoan metal-independent beta-galactoside-binding lectins: structure, function and molecular evolution. *Glycobiology* **1993,** *3* (4), 297-304.
31. Yang, R.-Y.; Hsu, D. K.; LIu, F.-T., Expression of galectin-3 modulates T-cell growth and apoptosis. *Proc. Natl. Acad. Sci. U.S.A.* **1996,** *93* (13), 6737-6742.
32. Nakahara, S.; Oka, N.; Raz, A., On the role of galectin-3 in cancer apoptosis. *Apoptosis* **2005,** *10*, 267-275.
33. Nangia-Makker, P.; Nakahara, S.; Hogan, V.; Raz, A., Galectin-3 in apoptosis, a novel therapeutic target. *J. Bioenerg. Biomembr.* **2007,** *39*, 79-84.
34. Capone, E.; Iacobelli, S.; Sala, G., Role of galectin 3 binding protein in cancer progression: A potential novel therapeutic target. *J. Transl. Med.* **2021,** *19* (1), 1-18.
35. Newlaczyl, A. U.; Yu, L.-G., Galectin-3–a jack-of-all-trades in cancer. *Cancer Lett.* **2011,** *313* (2), 123-128.
36. Ahmed, H.; AlSadek, D. M., Galectin-3 as a potential target to prevent cancer metastasis. *Clin. Med. Insights Oncol.* **2015,** *9*, CMO. S29462.
37. Henderson, N. C.; Sethi, T., The regulation of inflammation by galectin-3. *Immunol. Rev.* **2009,** *230* (1), 160-171.
38. de Oliveira, F. L.; Gatto, M.; Bassi, N.; Luisetto, R.; Ghirardello, A.; Punzi, L.; Doria, A., Galectin-3 in autoimmunity and autoimmune diseases. *Exp. Biol. Med. (Maywood N.J.)* **2015,** *240* (8), 1019-1028.
39. Díaz-Alvarez, L.; Ortega, E., The many roles of galectin-3, a multifaceted molecule, in innate immune responses against pathogens. *Mediators Inflamm.* **2017,** *2017*.
40. Ruvolo, P. P., Galectin 3 as a guardian of the tumor microenvironment. *Biochim. Biophys. Acta (BBA)-Mol. Cell Res.* **2016,** *1863* (3), 427-437.
41. Fortuna-Costa, A.; Gomes, A. M.; Kozlowski, E. O.; Stelling, M. P.; Pavão, M. S., Extracellular galectin-3 in tumor progression and metastasis. *Front. Oncol.* **2014,** *4*, 138.
42. Takenaka, Y.; Fukumori, T.; Raz, A., Galectin-3 and metastasis. *Glycoconjugate J.* **2002,** *19*, 543-549.

43. Verma, R.; Riaz, J.; Mirandola, L.; Figueroa, J. A.; Radhi, S.; Konala, V.; Aulakh, A.; Yu, Y.; Nguyen, D. D. T.; Hardwick, F., Effect of galectin-3 inhibition on drug resistance, motility, invasion, and angiogenic potential in ovarian cancer. *Gynecol. Oncol.* **2014,** *135(3)*, 573–579.
44. Jarvis, G. A.; Mirandola, L.; Yuefei, Y.; Cobos, E.; Chiriva-Internati, M.; John, C. M., Galectin-3C: human lectin for treatment of cancer. In *Galectins and Disease Implications for Targeted Therapeutics*, ACS Publications: 2012; pp 195-232.
45. Mirandola, L.; Nguyen, D. D.; Rahman, R. L.; Grizzi, F.; Yuefei, Y.; Figueroa, J. A.; Jenkins, M. R.; Cobos, E.; Chiriva-Internati, M., Anti-galectin-3 therapy: a new chance for multiple myeloma and ovarian cancer? *Int. Rev. Immunol.* **2014,** *33* (5), 417-427.
46. Seetharaman, J.; Kanigsberg, A.; Slaaby, R.; Leffler, H.; Barondes, S. H.; Rini, J. M., X-ray crystal structure of the human galectin-3 carbohydrate recognition domain at 2.1-A resolution. *J. Biol. Chem.* **1998,** *273* (21), 13047-52.
47. Knibbs, R. N.; Agrwal, N.; Wang, J. L.; Goldstein, I. J., Carbohydrate-binding protein 35. II. Analysis of the interaction of the recombinant polypeptide with saccharides. *J. Biol. Chem.* **1993,** *268* (20), 14940-7.
48. Peterson, K.; Kumar, R.; Stenström, O.; Verma, P.; Verma, P. R.; Håkansson, M.; Kahl-Knutsson, B.; Zetterberg, F.; Leffler, H.; Akke, M.; Logan, D. T.; Nilsson, U. J., Systematic tuning of fluoro-galectin-3 interactions provides thiodigalactoside derivatives with single-digit nm affinity and high selectivity. *J. Med. Chem.* **2018,** *61* (3), 1164-1175.
49. Verteramo, M. L.; Stenström, O.; Ignjatović, M. M.; Caldararu, O.; Olsson, M. A.; Manzoni, F.; Leffler, H.; Oksanen, E.; Logan, D. T.; Nilsson, U. J.; Ryde, U.; Akke, M., Interplay between conformational entropy and solvation entropy in protein-ligand binding. *J. Am. Chem. Soc.* **2019,** *141* (5), 2012-2026.
50. Saraboji, K.; Håkansson, M.; Genheden, S.; Diehl, C.; Qvist, J.; Weininger, U.; Nilsson, U. J.; Leffler, H.; Ryde, U.; Akke, M.; Logan, D. T., The carbohydrate-binding site in galectin-3 is preorganized to recognize a sugarlike framework of oxygens: ultra-high-resolution structures and water dynamics. *Biochem.* **2012,** *51* (1), 296-306.
51. Hou, G.; Suiter, C. L.; Yan, S.; Zhang, H.; Polenova, T., Magic angle spinning NMR studies of protein assemblies: Recent advances in methodology and applications. *Annu. Rep. NMR Spectrosc.* **2013,** *80*, 293-357.
52. Hou, G.; Byeon, I.-J. L.; Ahn, J.; Gronenborn, A. M.; Polenova, T., Recoupling of chemical shift anisotropy by R-symmetry sequences in magic angle spinning NMR spectroscopy. *J. Chem. Phys.* **2012,** *137* (13).
53. Kraus, J.; Gupta, R.; Yehl, J.; Lu, M.; Case, D. A.; Gronenborn, A. M.; Akke, M.; Polenova, T., Chemical shifts of the carbohydrate binding domain of galectin-3 from magic angle spinning NMR and hybrid quantum mechanics/molecular mechanics calculations. *J. Phys. Chem. B* **2018,** *122* (11), 2931-2939.
54. Frey, M.; DiVerdi, J.; Opella, S., Dynamics of phenylalanine in the solid state by NMR. *J. Am. Chem. Soc.* **1985,** *107* (25), 7311-7315.
55. Porat-Dahlerbruch, G.; Struppe, J.; Quinn, C. M.; Gronenborn, A. M.; Polenova, T., ^{19}F fast MAS (60–111 kHz) dipolar and scalar based correlation spectroscopy of organic molecules and pharmaceutical formulations. *J. Magn. Reson.* **2022,** *122*, 101831.
56. Porat-Dahlerbruch, G.; Struppe, J.; Quinn, C. M.; Gronenborn, A. M.; Polenova, T., Determination of accurate ^{19}F chemical shift tensors with R-symmetry recoupling at high MAS frequencies (60–100 kHz). *J. Magn. Reson.* **2022,** *340*, 107227.
57. Diehl, C.; Genheden, S.; Modig, K.; Ryde, U.; Akke, M., Conformational entropy changes upon lactose binding to the carbohydrate recognition domain of galectin-3. *J. Biomol. NMR* **2009,** *45* (1-2), 157-69.

58. Diehl, C.; Engström, O.; Delaine, T.; Håkansson, M.; Genheden, S.; Modig, K.; Leffler, H.; Ryde, U.; Nilsson, U. J.; Akke, M., Protein flexibility and conformational entropy in ligand design targeting the carbohydrate recognition domain of galectin-3. *J. Am. Chem. Soc.* **2010,** *132* (41), 14577-89.
59. Bennett, A. E.; Rienstra, C. M.; Auger, M.; Lakshmi, K.; Griffin, R. G., Heteronuclear decoupling in rotating solids. *J. Chem. Phys.* **1995,** *103* (16), 6951-6958.
60. Shaka, A.; Keeler, J.; Frenkiel, T.; Freeman, R., An improved sequence for broadband decoupling: WALTZ-16. *J. Magn. Reson.* **1983,** *52* (2), 335-338.
61. Barbet-Massin, E.; Pell, A. J.; Retel, J. S.; Andreas, L. B.; Jaudzems, K.; Franks, W. T.; Nieuwkoop, A. J.; Hiller, M.; Higman, V.; Guerry, P.; Bertarello, A.; Knight, M. J.; Felletti, M.; Le Marchand, T.; Kotelovica, S.; Akopjana, I.; Tars, K.; Stoppini, M.; Bellotti, V.; Bolognesi, M.; Ricagno, S.; Chou, J. J.; Griffin, R. G.; Oschkinat, H.; Lesage, A.; Emsley, L.; Herrmann, T.; Pintacuda, G., Rapid proton-detected NMR assignment for proteins with fast magic angle spinning. *J. Am. Chem. Soc.* **2014,** *136* (35), 12489-97.
62. Thurber, K. R.; Tycko, R., Measurement of sample temperatures under magic-angle spinning from the chemical shift and spin-lattice relaxation rate of ^{79}Br in KBr powder. *J. Magn. Reson.* **2009,** *196* (1), 84-87.
63. Hahn, E. L., An accurate nuclear magnetic resonance method for measuring spin-lattice relaxation times. *Phys. Rev.* **1949,** *76* (1), 145.
64. Delaglio, F.; Grzesiek, S.; Vuister, G. W.; Zhu, G.; Pfeifer, J.; Bax, A., NMRPipe: a multidimensional spectral processing system based on UNIX pipes. *J. Biomol. NMR* **1995,** *6* (3), 277-93.
65. Goddard, T.; Kneller, D., SPARKY 3 (San Francisco: University of California). 2004.
66. Tošner, Z.; Andersen, R.; Stevensson, B.; Edén, M.; Nielsen, N. C.; Vosegaard, T., Computer-intensive simulation of solid-state NMR experiments using SIMPSON. *J. Magn. Reson.* **2014,** *246*, 79-93.
67. Vosegaard, T.; Malmendal, A.; Nielsen, N. C., The flexibility of SIMPSON and SIMMOL for numerical simulations in solid-and liquid-state NMR spectroscopy. *Monatsh. Chem./Chem. Mon.* **2002,** *133* (12), 1555-1574.
68. Bak, M.; Rasmussen, J. T.; Nielsen, N. C., SIMPSON: a general simulation program for solid-state NMR spectroscopy. 2000. *J. Magn. Reson.* **2011,** *213* (2), 366-400.

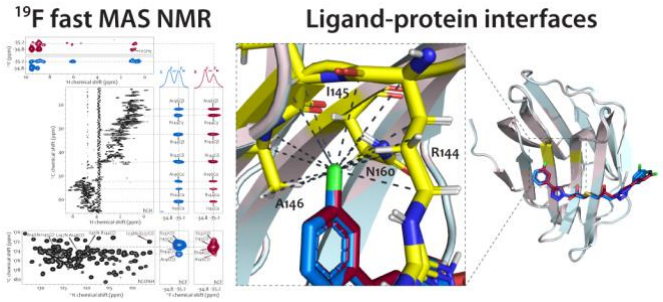

Table of Contents artwork